Feedback stabilization of vortex position near a deformable foil in a uniform flow using camber control

Rose Gebhardt
Department of Aerospace Engineering
University of Maryland
College Park, Maryland, USA
rgebhard@umd.edu

Derek A. Paley
Department of Aerospace Engineering
and Institute for Systems Research
University of Maryland
College Park, Maryland, USA
dpaley@umd.edu

***Abstract*—This paper presents a feedback control design that stabilizes the position of a drifting vortex in a freestream over a deformable Joukowski foil using camber control. We derive the dynamics of a point vortex in flow around a Joukowski foil using a potential flow model and provide numerical analysis of the number, stability, and controllability of open-loop equilibrium points of the vortex-foil system. We show that the position of a point vortex can effectively be stabilized using a full-state feedback camber control law while maintaining the validity of the dynamics model. We present sample stable and unstable trajectories found using closed-loop control along with a visualization of the region of convergence.**

***Index Terms*—vortex dynamics, foil deformations, feedback control**

I. Introduction

Biologically inspired autonomous underwater vehicles (AUVs) have certain advantages over typical propeller-based AUVs. Robotic fish are stealthier due to their low acoustic signature and inconspicuous wake structure, which can be important for defense applications [1]. In particular, bio-inspired locomotion improves efficiency, which enables longer operation times. The dynamics of a swimmer, particularly carangiform fish, can be modeled by a deformable Joukowski foil [2], which has a profile similar to a fish, and locomotion of this deformable body can be achieved through time-varying changes in the shape parameters [3], [4].

Drifting vortices can appear in a freestream in the wake of an oscillating or flapping bluff body or foil. These have impacts on the lift and circulation of an object in freestream. In particular, if the object is a moving body, vortices can provide hydrodynamic benefits that enable the body to move faster or with better energy efficiency [5]. Prior work has studied low-dimensional models of vortical flow fields and applied feedback control in order to stabilize vortices. A model-based observer, using bio-inspired distributed flow sensing and a feedback controller have been designed for a rigid Joukowski foil in a Kármán vortex street [6]. Adaptive control of real singularity strengths to stabilize formations of virtual vortices has been derived [7]. A vortex in freestream around a cylinder can be stabilized by controlling the cylinder's velocity in the plane [8].

This paper describes the design of a control system used to stabilize the position of a drifting point vortex in a freestream near a swimmer using feedback control of the swimmer's shape. The swimmer is modeled by a deformable Joukowski foil and the control input is the shape parameter that affects camber. In ongoing work, we seek to extend the stabilization results to trajectory tracking.

The contributions of this paper are (1) a low-dimensional model of a flexible foil in vortical flow to replicate bio-inspired locomotion; (2) numerical analysis of the open-loop model including a study of the effect of the drifting vortex strength and the degree of camber on the number and stability of equilibrium points; and (3) a full-state linear control law computed numerically to stabilize an arbitrary equilibrium point and the corresponding analysis of its region of convergence. This work has applications in bio-inspired underwater vehicles and aerodynamics.

The outline of this paper is as follows. Section II summarizes the dynamics and control approach of prior work on stabilizing a point vortex in flow around a cylinder. Section III uses these results to derive the dynamics of a vortex near a streamlined foil. Section IV introduces the control inputs, describes a parameter study to analyze the impact of nominal values of the control inputs on the location of equilibrium points, and provides a feedback control law to stabilize vortex position. Section V summarizes key results and discusses ongoing work.

II. Background

Prior work has accomplished the closely-related task of stabilizing the position of a drifting vortex in freestream around a cylinder by controlling the heaving and surging velocities of the cylinder [8]. The steps taken to derive the dynamics and control of the vortex-cylinder model along with

an analysis of the open-loop and closed-loop dynamics are summarized in this section. For more details on the derivation of the fluid dynamics, refer to [9] and [10].

A. Dynamics of a point vortex around a cylinder in freestream

Aerodynamic surfaces are designed to have low drag and a relatively thin boundary layer, so the effect of the boundary layer may be ignored [11]. The ideal flow assumption applies if the flow is irrotational except at discrete points and has a sufficiently low Mach number to be considered incompressible. The flow may then be modeled by a complex potential function, $F(\zeta)$, where $\zeta = \zeta_1 + i\zeta_2$.

The potential function has real and imaginary components, i.e., $F(\zeta) = F(\zeta_1 + i\zeta_2) = \Phi(\zeta_1, \zeta_2) + i\Psi(\zeta_1, \zeta_2)$, where $\Phi(\zeta)$ and $\Psi(\zeta)$ are the real scalar-valued velocity and streamline functions, respectively. Differentiating $F(\zeta)$ gives the complex conjugate velocity [11]

$$\frac{dF}{d\zeta} = \frac{\partial \Phi}{\partial \zeta_1} - i\frac{\partial \Phi}{\partial \zeta_2} = \dot{\zeta}_1 - i\dot{\zeta}_2.$$

Consider a cylinder of radius r_0 centered at ζ_0 in a freestream of strength u_∞. The circulation Γ_0 around the cylinder is a free parameter modeled by a point vortex at ζ_0 with strength Γ_0. We model the motion of a point vortex near the cylinder with circulation Γ_v, shown in Figure 1. The interaction between the cylinder and the point vortex is represented by an image vortex. This image vortex has the same circulation as the actual vortex acting in the opposite direction; it is located at [8]

$$\zeta_{im} = \zeta_0 + \frac{r_0^2}{(\zeta_v - \zeta_0)^*}.$$

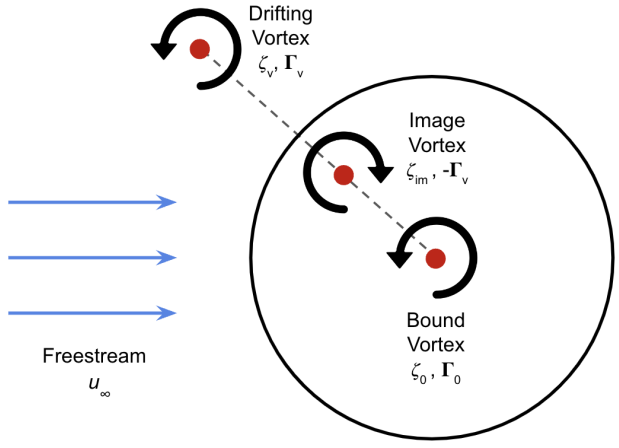

Fig. 1: Fluid model of a drifting vortex around a cylinder [8]

Using linearity of solutions of Laplace's equation and the Milne-Thompson circle theorem [10], we find that when the drifting point vortex is at position ζ_v, the complex potential function for a particle in the system is

$$F(\zeta) = u_\infty^* \zeta + \left(\frac{u_\infty r_0^2}{\zeta - \zeta_0}\right) + \frac{\Gamma_0}{2\pi i}\log(\zeta - \zeta_0) - \frac{\Gamma_v}{2\pi i}\log(\zeta - \zeta_{im}) + \frac{\Gamma_v}{2\pi i}\log(\zeta - \zeta_v). \quad (1)$$

A point vortex is convected by the portion of the flow excluding its own contribution, so the complex potential that describes its motion is

$$F^{-v}(\zeta) = u_\infty^* \zeta + \left(\frac{u_\infty r_0^2}{\zeta - \zeta_0}\right) + \frac{\Gamma_0}{2\pi i}\log(\zeta - \zeta_0) - \frac{\Gamma_v}{2\pi i}\log(\zeta - \zeta_{im}) \quad (2)$$

and the complex conjugate of the vortex velocity is

$$\dot{\zeta}_v = u_\infty - u_\infty^* \left(\frac{r_0^2}{([\zeta_v - \zeta_0]^2)^*}\right) + \frac{i\Gamma_0}{2\pi}\left(\frac{\zeta_v - \zeta_0}{|\zeta_v - \zeta_0|^2}\right) - \frac{i\Gamma_v}{2\pi}\left(\frac{\zeta_v - \zeta_0}{|\zeta_v - \zeta_0|^2 - r_0^2}\right). \quad (3)$$

Now let $\zeta_v = \zeta_1 + i\zeta_2$ be the position of the vortex in the complex plane and break the prior equation into its real and imaginary components, which yields a two-dimension nonlinear state-space system. In prior work [8], the length and time scales were normalized by setting $r_0 = 1$, $u_0 = 1$, $u_\infty = (1 - u_1 - iu_2)u_0$, $\zeta_v = r_0(\zeta_1 + i\zeta_2)$, $\Gamma_0 = 2\pi r_0 u_0 \sigma_0$, and $\Gamma_v = 2\pi r_0 u_0 \sigma_v$. These choices non-dimensionalize the state vector and introduce non-dimensional control inputs u_1 and u_2, corresponding to the normalized velocity of the cylinder in the ζ_1 and ζ_2 directions, respectively. The two remaining system parameters are σ_0 and σ_v. The state-space system may be written as [8]

$$\dot{\zeta}_1 = (1 - u_1)\left[\frac{\zeta_2^2 - \zeta_1^2}{(\zeta_1^2 + \zeta_2^2)^2} + 1\right] - u_2\left[\frac{2\zeta_1\zeta_2}{(\zeta_1^2 + \zeta_2^2)^2}\right] - \sigma_0\left[\frac{\zeta_2}{\zeta_1^2 + \zeta_2^2}\right] + \sigma_v\left[\frac{\zeta_2}{\zeta_1^2 + \zeta_2^2 - 1}\right]$$

$$\dot{\zeta}_2 = (1 - u_1)\left[\frac{-2\zeta_1\zeta_2}{(\zeta_1^2 + \zeta_2^2)^2}\right] + u_2\left[\frac{\zeta_2^2 - \zeta_1^2}{(\zeta_1^2 + \zeta_2^2)^2} - 1\right] + \sigma_0\left[\frac{\zeta_1}{\zeta_1^2 + \zeta_2^2}\right] - \sigma_v\left[\frac{\zeta_1}{\zeta_1^2 + \zeta_2^2 - 1}\right].$$

The equilibrium points, $\tilde{\zeta}_v = \tilde{\zeta}_1 + i\tilde{\zeta}_2$, of this system are found by setting $\dot{\zeta}_1 = \dot{\zeta}_2 = 0$. We get $\tilde{\zeta}_1 = 0$ for all equilibrium points and possible values of $\tilde{\zeta}_2$ are roots of the polynomial [8]

$$\tilde{\zeta}_2^{\,4} + (\sigma_v - \sigma_0)\tilde{\zeta}_2^{\,3} + \sigma_0\tilde{\zeta}_2 - 1 = 0.$$

Furthermore, there will always be one equilibrium point in the domain (-1,1), which is located inside the cylinder and therefore invalid, and there will always be one equilibrium point in the domain (-∞,-1), which is a saddle point. Depending on the system parameters, there can be zero, one,

or two equilibrium points in the domain (1,∞). If there are two equilibrium points, they will be a saddle point and a center point. As the parameters of the system change, there can be a saddle-center collision leading to one equilibrium point above the cylinder. This point is not of much interest, however, since it occurs with zero volume in the parameter space [8].

Figure 2 shows the velocity field and sample trajectories of a vortex on the left and, on the right, the number of equilibrium points of a representative configuration of the system as the bound vortex strength changes. Figure 2 has parameters $\sigma_v = 2$ and $\sigma_0 = 6$, yielding three equilibrium points.

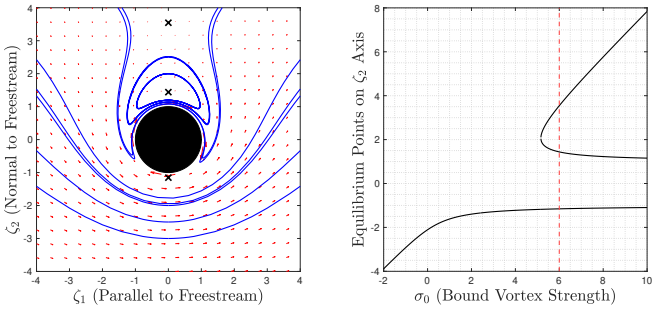

Fig. 2: The cylinder-vortex system with $\sigma_v = 2$ yields three equilibrium points for $\sigma_0 = 6$

B. Feedback stabilization control of a vortex near a cylinder

The control inputs u_1 and u_2 in the cylinder-vortex system are the non-dimensionalized velocities of the cylinder in the ζ_1 and ζ_2 directions, which correspond to surging and heaving. A closed-loop controller that stabilizes the system in the neighborhood of an equilibrium point is derived by linearizing the state-space equations about any of the equilibrium points $\tilde{x} = \begin{bmatrix} 0 \\ \tilde{x_2} \end{bmatrix}$ and $\tilde{u} = \begin{bmatrix} u_1 \\ u_2 \end{bmatrix} = \begin{bmatrix} 0 \\ 0 \end{bmatrix}$.

To obtain a linear state-space system, we compute the Jacobians

$$A_{ij} = \left.\frac{\partial \dot{x_i}}{\partial x_j}\right|_{(\tilde{x},\tilde{u})} \quad \text{and} \quad B_{ij} = \left.\frac{\partial \dot{x_i}}{\partial u_j}\right|_{(\tilde{x},\tilde{u})}.$$

These evaluate to the A and B matrices

$$A = \begin{bmatrix} 0 & \frac{\sigma_0}{\tilde{x_2}^2} - \frac{\sigma_v(\tilde{x_2}^2+1)}{(\tilde{x_2}^2-1)^2} - \frac{2}{\tilde{x_2}^3} \\ \frac{\sigma_0}{\tilde{x_2}^2} - \frac{\sigma_v}{(\tilde{x_2}^2-1)^2} - \frac{2}{\tilde{x_2}^3} & 0 \end{bmatrix}$$

$$B = \begin{bmatrix} -1 - \frac{1}{\tilde{x_2}} & 0 \\ 0 & -1 + \frac{1}{\tilde{x_2}} \end{bmatrix},$$

which yields the linear time-invariant system [8]

$$\begin{bmatrix} \dot{x_1} \\ \dot{x_2} \end{bmatrix} = A \begin{bmatrix} x_1 \\ x_2 - \tilde{x_2} \end{bmatrix} + B \begin{bmatrix} u_1 \\ u_2 \end{bmatrix}$$

and the state-feedback control

$$u = \begin{bmatrix} u_1 \\ u_2 \end{bmatrix} = - \begin{bmatrix} k_{11} & k_{12} \\ k_{21} & k_{22} \end{bmatrix} \begin{bmatrix} x_1 \\ x_2 - \tilde{x_2} \end{bmatrix} = -K(x - \tilde{x}).$$

In order for the closed-loop system to be locally exponentially stable, the matrix $A_{cl} = A - BK$ must be Hurwitz. This is equivalent to the gain values satisfying the inequalities [8]

$$k_{11}k_{22} - \left(k_{12} + \frac{1}{\tilde{x_2}} - \frac{2\sigma_v \tilde{x_2}}{(\tilde{x_2}^2 - 1)^3}\right)\left(k_{21} + \frac{1}{\tilde{x_2}}\right) > 0$$

and

$$k_{11} + k_{22} + \frac{k_{11} - k_{22}}{\tilde{x_2}^2} < 0.$$

It is therefore possible to achieve exponential stability with surging gains only ($k_{21} = k_{22} = 0$), heaving gains only ($k_{11} = k_{12} = 0$), x_1-feedback only ($k_{12} = k_{22} = 0$), or x_2-feedback only ($k_{11} = k_{21} = 0$), which is a useful design consideration for systems with actuation or sensing limitations.

III. Dynamics of a Vortex Near a Deformable Foil

The previous work is extended here to find the dynamics of a point vortex around a deformable body, which can be represented by the image of a circle under the Joukowski transform. In this section, none of the parameters are non-dimensionalized.

A. Derivation of vortex equations of motion

The Joukowski transform is a conformal map that transforms circles to a range of airfoil profiles, as shown in Figure 3 . The map is defined by [9]

$$z = g(\zeta) = \zeta + \frac{k^2}{\zeta},$$

where k is fixed according to the relation $|\zeta_0 - k| = r_0$. Under this map, the real component of ζ_0 changes the thickness of the foil and the imaginary component changes the camber.

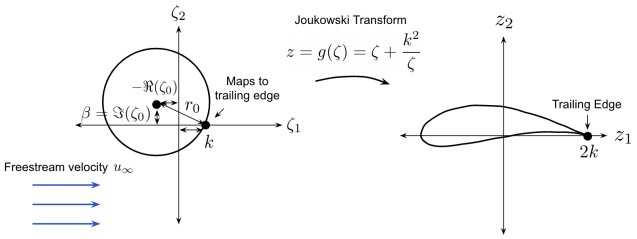

Fig. 3: Joukowski mapping applied to a cylinder

The complex representation of ideal flow permits flow solutions to be modified by conformal mapping. We map the complex potential $F(\zeta)$ in the ζ-plane to a complex potential in the z-plane by the equation

$$F(\zeta) = H(z) = H(g(\zeta)).$$

We obtain the complex velocity in the z-plane by differentiating [11], i.e.,

$$\frac{dF}{d\zeta} = \frac{dH}{dz}\frac{dz}{d\zeta} \quad \Longrightarrow \quad \frac{dH}{dz} = \frac{1}{g'(\zeta)}\frac{dF}{d\zeta}.$$

However, this equation does not hold for the singularity at the convecting vortex because the flow is not irrotational. Instead, the convection velocity is corrected to be [11]

$$\dot{z_v}^* = \lim_{\zeta \to \zeta_v} \left[\frac{1}{g'(\zeta)} \frac{dF^{-v}}{d\zeta} + \frac{i\Gamma_v}{4\pi} \frac{g''(\zeta)}{g'(\zeta)^2} \right]$$

which can be rewritten as

$$\dot{z_v}^* = \frac{1}{g'(\zeta_v)} \left[\left(\frac{dF^{-v}}{d\zeta} \right) \Bigg|_{\zeta=\zeta_v} + \lim_{\zeta \to \zeta_v} \left(\frac{i\Gamma_v}{4\pi} \frac{g''(\zeta)}{g'(\zeta)} \right) \right].$$

The first term in the brackets is the velocity field of the cylinder system defined in (3). The second term in this equation is the Routh correction term, given by [11]

$$R = \frac{\Gamma_v}{4\pi i} \frac{k^2}{\zeta_v(\zeta_v^2 - k^2)}.$$

The complex velocity written in terms of ζ is

$$\dot{z_v} = \frac{1}{g'(\zeta_v)^*} \left(\dot{\zeta_v}^* + R^* \right). \tag{4}$$

The inverse mapping of the Joukowski transform is $\zeta(z) = \frac{1}{2}\left(z + \sqrt{z^2 - \text{sign}(\text{Re}(z))4k^2}\right)$, which gives us the inverse transform of each component [12]

$$\zeta_1 = \frac{z_1}{2} \pm \left[(z_1^2 - z_2^2 - 4k^2)^2 + 4z_1^2 z_2^2\right]^{\frac{1}{4}} \cos\left(\frac{1}{2}\tan^{-1}\left(\frac{2z_1 z_2}{z_1^2 - z_2^2 - 4k^2}\right)\right)$$

and

$$\zeta_2 = \frac{z_2}{2} \pm \left[(z_1^2 - z_2^2 - 4k^2)^2 + 4z_1^2 z_2^2\right]^{\frac{1}{4}} \sin\left(\frac{1}{2}\tan^{-1}\left(\frac{2z_1 z_2}{z_1^2 - z_2^2 - 4k^2}\right)\right)$$

Thus, it is possible to expand $\dot{z}_v$ in terms of z_1 and z_2. The full expansion is omitted for brevity.

Unlike the cylinder case, the circulation around the cylinder must satisfy the Kutta condition, which ensures that the velocity at the trailing edge is zero. Γ_0 therefore becomes fixed according to the configuration of the cylinder and the drifting vortex according to the equation [8]

$$\left(\frac{dF}{d\zeta} \right) \Bigg|_{\zeta=k} = 0,$$

which is expanded to

$$u_\infty - \frac{u_\infty r_0^2}{(k-\zeta_0)^2} + \frac{\Gamma_0}{2\pi i}\left(\frac{1}{k-\zeta_0}\right) + \frac{\Gamma_v}{2\pi i}\left(\frac{|\zeta_v - \zeta_0|^2 - r_0^2}{(k-\zeta_v)[(k-\zeta_0)(\zeta_v-\zeta_0)^\star - r_0^2]}\right) = 0.$$

Solving for Γ_0 yields

$$\Gamma_0 = \frac{2\pi i u_\infty r_0^2}{k-\zeta_0} - 2\pi i(k-\zeta_0)u_\infty - \Gamma_v\left(\frac{|\zeta_v-\zeta_0|^2 - r_0^2}{(k-\zeta_v)\left[(\zeta_v-\zeta_0)^\star - \frac{r_0^2}{k-\zeta_0}\right]}\right)$$

which simplifies to

$$\Gamma_0 = \Gamma_v\left(\frac{|\zeta_v-\zeta_0|^2 + r_0^2}{|\zeta_v - k|^2}\right) - 4\pi u_\infty \text{Im}(k-\zeta_0).$$

Substituting this value into (4) yields the complete two-dimensional equations of motion of the drifting vortex.

IV. Position control of a vortex near a foil

Under the Joukowski mapping, the control input of surging corresponds to changes in the foil camber and the control input of heaving corresponds to changes in foil thickness. The following section discusses the restrictions on the new control inputs, the effect on equilibrium points of the free parameters and nominal control gains, and a feedback control law used to stabilize vortex dynamics at these points.

A. Parameter constraints and assumptions

Consider a foil generated by a cylinder centered at $\zeta_0 = r_0(\delta + i\beta)$ with radius r_0; the control inputs for the cylinder inputs are the rate of change of δ, the thickness parameter, and β, the camber parameter. However, for the foil system, the control inputs must be altered for the model to remain a valid representation of a deforming foil.

First, to best model an actual flexible foil, the direction and the area of the foil should be kept constant. The direction the foil is pointing is determined by $\text{sign}(\delta)$ and the area A is given by [9]

$$A = \pi r_0^2\left(1 - \frac{k^4}{(r_0^2 - |\zeta_0|^2)^2}\right).$$

Assuming $\delta < 0$ correctly models the direction of the foil when $u_\infty \geq 0$; from the relation $|\zeta_0 - k| = r_0$ [9], we get $k = r_0(\delta + \sqrt{1-\beta^2})$. The area of the foil is a function of r_0, β, and δ. Since r_0 is a constant parameter, the only way to keep the area constant is to relate β and δ. Given a nominal value of the area, A_0, we fix δ given β according to

$$\delta = \left(\frac{\sqrt{\pi r_0^2 - A_0} - \sqrt{\pi r_0^2}}{\sqrt{\pi r_0^2 - A_0} + \sqrt{\pi r_0^2}}\right)\sqrt{1-\beta^2}.$$

So, unlike the cylinder system, which has two inputs, the foil system has only one control input, the camber parameter β. Furthermore, the input is a displacement rather than a velocity. A few additional restrictions still must be placed on this input to maintain the validity of the potential flow model.

The first limitation on the camber parameter β is due to the fact that, if the cylinder does not enclose the origin, the Joukowski transform does not map to a closed contour [9]. So $r_0^2(\beta^2 + \delta^2) < 1$ has to be satisfied at all times. The maximum absolute magnitude of β that satisfies this limitation depends on A_0.

An even more restrictive limitation on β is caused by the potential flow model, which loses validity if the angle of attack of a foil is greater than 15 degrees [12]. Camber in the foil creates an angle between the flow stream and the leading edge of the foil given by $\arcsin(\beta/r_0)$. Therefore, the

maximum allowable magnitude of β to satisfy this limitation is $r_0 \sin(15°)$. To preserve model validity, the control input is saturated at $\beta = \pm r_0 \sin(15°) \approx 0.259 r_0$.

Lastly, in order to restrict the number of free parameters, we normalize the cylinder radius and the freestream velocity to $r_0 = 1$ and $u_0 = 1$. The remaining two free parameters of the system are the nominal thickness δ_0, which is the thickness that yields the nominal area A_0 when the foil has zero camber, and the circulation of the drifting vortex Γ_v.

B. Equilibrium points and bifurcations

Unlike the cylinder system, it is not feasible to find a closed-form expression for the location of the equilibrium points around the foil. This process is instead performed numerically.

The nullclines of the vector field defined by (4) are given by the solutions to the differential equations $\dot{z_1}(z_1, z_2) = 0$ and $\dot{z_2}(z_1, z_2) = 0$. Once computed, the intersection points of these solutions are the equilibrium points of the foil system.

This method is illustrated in Figure 4. In both figures, the free parameters are $\Gamma_v = -400$ and $\delta_0 = -0.2$, so the circulation of the drifting vortex and the area of the foil are the same. In Figure 4a, the camber input parameter is $\beta = -0.2$, and in Figure 4b, $\beta = 0.0$. The two subplots show the two nullcline manifolds with the red and blue lines, the intersection points with black crosses, and the shape of the foil. As enforced by the Kutta condition, there is an equilibrium point at the trailing edge of both configurations, but depending on the values of β, there are an additional two or four equilibrium points near the foil. As the camber parameter varies, two of these points collide and vanish.

The effect of the configuration in the β-Γ_v parameter space is shown in Figure 5. The shaded areas are where five equilibrium points appear and the unshaded areas are where there are only three. There is rotational symmetry about the origin for where two of the equilibrium points bifurcate in this space.

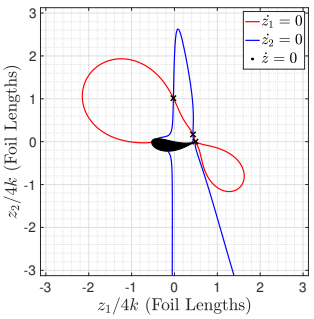

(a) Foil system with $\Gamma_v = -400$ and $\beta = -0.2$: three equilibrium points

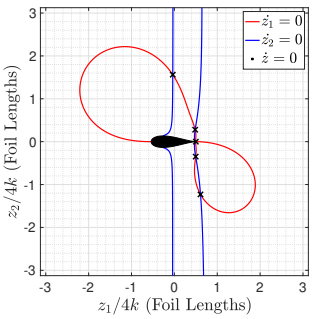

(b) Foil system with $\Gamma_v = -400$ and $\beta = 0$: five equilibrium points

Fig. 4: Shape of nullcline manifolds and location of equilibrium points for various nominal camber values

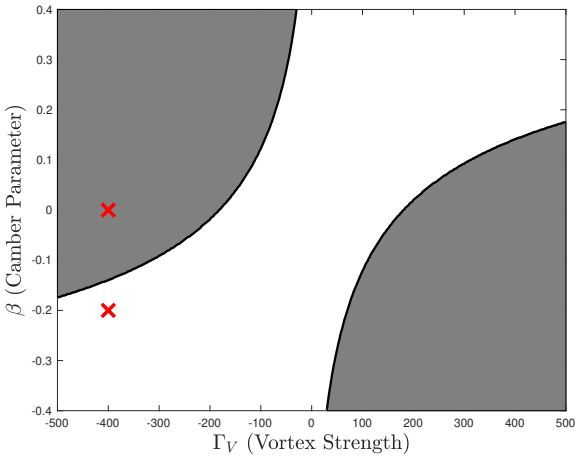

Fig. 5: Number of equilibrium points in the parameter space: shaded areas indicate five equilibrium points and unshaded areas indicate three equilibrium points; red markers correspond to configurations shown in Figures 4a (bottom) and 4b (top)

In addition to the location of the equilibrium points, we also determine the stability, local behavior, and controllability of each point. To determine these characteristics, the Jacobians at the equilibrium points are computed numerically using small difference approximations, that is

$$A = \begin{bmatrix} \frac{\partial \dot{z_1}}{\partial z_1} & \frac{\partial \dot{z_1}}{\partial z_2} \\ \frac{\partial \dot{z_2}}{\partial z_1} & \frac{\partial \dot{z_2}}{\partial z_2} \end{bmatrix}_{\tilde{z},\tilde{u}} \approx \frac{1}{2h} \begin{bmatrix} \dot{z_1}(\tilde{z_1}+h, \tilde{z_2}) - \dot{z_1}(\tilde{z_1}-h, \tilde{z_2}) & \dot{z_2}(\tilde{z_1}+h, \tilde{z_2}) - \dot{z_2}(\tilde{z_1}-h, \tilde{z_2}) \\ \dot{z_1}(\tilde{z_1}, \tilde{z_2}+h) - \dot{z_1}(\tilde{z_1}, \tilde{z_2}-h) & \dot{z_2}(\tilde{z_1}, \tilde{z_2}+h) - \dot{z_2}(\tilde{z_1}, \tilde{z_2}-h) \end{bmatrix}_{\tilde{z},\tilde{u}}$$

$$B = \begin{bmatrix} \frac{\partial \dot{z_1}}{\partial u} \\ \frac{\partial \dot{z_2}}{\partial u} \end{bmatrix}_{\tilde{z},\tilde{u}} \approx \frac{1}{2h} \begin{bmatrix} \dot{z_1}(\tilde{u}+h) - \dot{z_1}(\tilde{u}-h) \\ \dot{z_2}(\tilde{u}+h) - \dot{z_2}(\tilde{u}-h) \end{bmatrix}_{\tilde{z},\tilde{u}},$$

where $h \ll 1$ and the input $u = \beta$.

First, the behavior near each equilibrium point is classified based on the trace and determinant of A. At the trailing edge, the values in A diverge giving invalid classifications. However, each of the other equilibrium points consistently has a negative determinant, implying they are each saddles and therefore unstable.

Next the controllability of each point is determined by the rank of the controllability matrix $\mathcal{C} = [B|AB]$. Again, at the trailing edge the Jacobians are ill-defined and controllability cannot be classified. However, each of the other equilibrium points has a full-rank controllability matrix and can thus be stabilized in some region around the point.

C. State-feedback stabilization control of a foil

This section discusses the feedback control law developed for equilibrium points not on the trailing edge. Instead of

looking for equations governing individual gain parameters, which was done for the control law developed for vortices near a cylinder, a full-state control law is derived using a linear-quadratic regulator (LQR).

An LQR design avoids the problem of finding a full closed-form expression for the Jacobians and symbolically computing the trace and determinant. Although this was possible for the dynamics near a cylinder, it is intractable with the inverse Joukowski transform applied for dynamics near the foil. An LQR design also minimizes the control input, which is important because, unlike the cylinder case where no limitations were placed upon the surging and heaving inputs, the input may not exceed $\pm r_0 \sin(15°)$ and still preserve model validity.

The gain values found with LQR optimize the cost function $J = \int_0^\infty [z^T Q z + u^T R u] dt$. To minimize the magnitude of the control input, the R value should be one or more orders of magnitude larger than the Q values. We apply gain values K found using $Q = \mathbb{I}^{2\times 2}$ and $R = 1000$ and apply the saturation nonlinearity

$$u(t) = \begin{cases} -\sin(15°) & u_{eq} - K z_{eq} < -\sin(15°) \\ u_{eq} - K z_{eq} & -\sin(15°) \leq u_{eq} - K z_{eq} \leq \sin(15°) \\ \sin(15°) & u_{eq} - K z_{eq} > \sin(15°) \end{cases}$$

The full results of this feedback law are shown in Figure 6. In this figure, the foil has zero camber and the system has the same parameter values and equilibrium points as Figure 4b. The subplots show the application of feedback to stabilize two of the four points near the foil. On the plot, the blue area shows the region of convergence for the particular equilibrium point, the red area shows the initial conditions for which the trajectories diverge, and the gray arrows indicate the closed-loop velocity field of the drifting vortex. Each figure shows three trajectories, two of which converge to the desired endpoint and one of which diverges, shown by the dashed line.

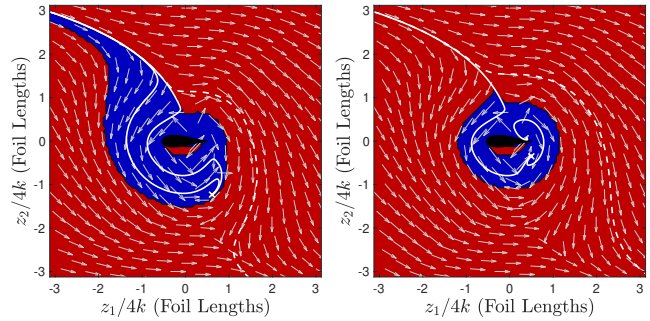

Fig. 6: Sample trajectories in the closed-loop foil system with $\Gamma_v = -400$, $\delta_0 = -0.2$, $\beta = 0$ linearized about a single equilibrium point. The uncambered foil is is shown for reference; the camber changes as a function of vortex position.

A characteristic of this configuration, also seen in several other configurations, is the appearance of stable manifolds in the state space. In Figure 6, these appear in the upper left and lower right corners. The size of the region of convergence changes drastically depending on the system parameters and choice of equilibrium point.

V. Conclusions

This paper derives the dynamics of a free vortex in freestream near a foil, describes a parameter study to characterize equilibrium points of the system, and develops an effective state-feedback stabilization control law that maintains the validity of the dynamics model. Ongoing work on this topic seeks a better characterization of the structure of the closed-loop system by finding the Lagrangian coherent structures of the trajectories and analyzing the fluid-structure interactions between the vortex and the foil. These interactions can generate lift and drag forces to the foil, enabling it to move relative to the flow.

References

[1] M. Sfakiotakis, D. M. Lane, and J. B. C. Davies, "Review of fish swimming modes for aquatic locomotion," *IEEE Journal of Oceanic Engineering*, vol. 24, no. 2, pp. 237–252, 1999.

[2] R. J. Mason, *Fluid locomotion and trajectory planning for shape-changing robots*. PhD thesis, 2003.

[3] "Self-propulsion of general deformable shapes in a perfect fluid," *Proceedings of the Royal Society of London. Series A: Mathematical and Physical Sciences*, vol. 442, pp. 273–299, Aug. 1993.

[4] E. Kanso, J. E. Marsden, C. W. Rowley, and J. B. Melli-Huber, "Locomotion of articulated bodies in a perfect fluid," *Journal of Nonlinear Science*, vol. 15, pp. 255–289, Aug. 2005.

[5] S. J. Lighthill, *Mathematical Biofluiddynamics*. Society for Industrial and Applied Mathematics, Jan. 1975.

[6] B. A. Free and D. A. Paley, "Model-based observer and feedback control design for a rigid joukowski foil in a Kármán vortex street," *Bioinspiration Biomimetics*, vol. 13, no. 3, p. 035001, 2018.

[7] F. D. Lagor and D. A. Paley, "Active singularities for multivehicle motion planning in an n-vortex system," in *Dynamic Data-Driven Environmental Systems Science*, pp. 334–346, Springer International Publishing, 2015.

[8] D. F. Gomez and D. A. Paley, "Closed-loop control of the position of a single vortex relative to an actuated cylinder," in *American Control Conference*, pp. 3563–3568, 2019.

[9] H. Xiong, *Geometric mechanics, ideal hydrodynamics, and the locomotion of planar shape-changing aquatic vehicles*. PhD thesis, 2007.

[10] L. M. Milne-Thomson, *Theoretical hydrodynamics*. Dover Publications, 1979.

[11] S. Glegg and W. Devenport, "The equations of fluid motion," in *Aeroacoustics of Low Mach Number Flows*, pp. 9–48, Elsevier, 2017.

[12] L. DeVries and D. A. Paley, "Observability-based optimization for flow sensing and control of an underwater vehicle in a uniform flowfield," in *American Control Conference*, IEEE, June 2013.